*J. Fluid Mech.* (2013), *vol.* 736, *pp.* 444–463.  
doi:10.1017/jfm.2013.538

# Similarity models for unsteady free convection flows along a differentially cooled horizontal surface

**Alan Shapiro**[1,2,†] **and Evgeni Fedorovich**[1]

[1]School of Meteorology, University of Oklahoma, Norman, OK 73072, USA

[2]Center for Analysis and Prediction of Storms, University of Oklahoma, Norman, OK 73072, USA

(Received 11 December 2012; revised 1 October 2013; accepted 7 October 2013;
first published online 7 November 2013)

A class of unsteady free convection flows over a differentially cooled horizontal surface is considered. The cooling, specified in terms of an imposed negative buoyancy or buoyancy flux, varies laterally as a step function with a single step change. As thermal boundary layers develop on either side of the step change, an intrinsically unsteady, boundary-layer-like flow arises in the transition zone between them. Self-similarity model solutions of the Boussinesq equations of motion, thermal energy, and mass conservation, within a boundary-layer approximation, are obtained for flows of unstratified fluids driven by a surface buoyancy or buoyancy flux, and flows of stably stratified fluids driven by a surface buoyancy flux. The motion is characterized by a shallow, primarily horizontal flow capped by a weak return flow. Stratification weakens the primary flow and strengthens the return flow. The flows intensify as the step change in surface forcing increases or as the Prandtl number decreases. Simple formulas are obtained for the propagation speeds, trajectories and the evolution of velocity maxima and other local extrema. Similarity-model predictions are verified through numerical simulations in which no boundary-layer approximations are made.

**Key words:** baroclinic flows, boundary layers, convection

## 1. Introduction

When a horizontal surface underlying a quiescent fluid is cooled, diffusion communicates the state of the surface to the fluid, and a statically stable thermal field develops. If the cooling varies along the surface, buoyancy variations arise in the fluid, and the associated pressure variations drive a shallow, primarily horizontal flow. Following Amin & Riley (1990), we refer to such flow types as horizontal free convection. A distinguishing feature of these flows is the action of the buoyancy force in a direction perpendicular to the principal motion. Although not studied as extensively as plumes, thermals, or convection flows along vertical surfaces, horizontal free convection flows are, nevertheless, ubiquitous. Horizontal free convection flows along cooled upward-facing horizontal surfaces or, equivalently, along

† Email address for correspondence: ashapiro@ou.edu

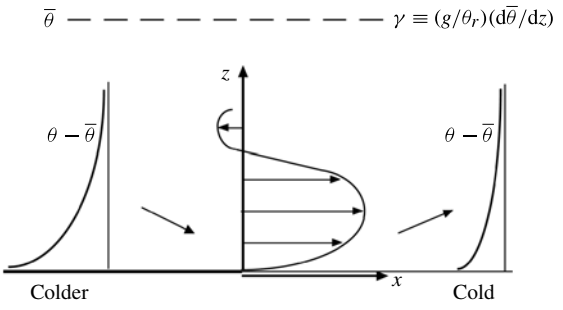


FIGURE 1. Schematic of a horizontal free convection flow in a stably stratified fluid. The motion is independent of the $y$ (into-page) coordinate.

heated downward-facing horizontal surfaces are of long-standing interest in the heat transfer community (reviewed in § 5.3.4 of Gebhart *et al.* 1988). In the atmosphere, differential cooling of the underlying surface gives rise to internal boundary layers, land breezes and other local circulations (Atkinson 1981; Garratt 1990; Simpson 1994). The role of surface heterogeneities in generating local circulations and promoting transport of heat, moisture, and contaminants is of fundamental interest for boundary-layer meteorology, air pollution meteorology, and numerical weather prediction.

Although numerical simulations are standard in studies of free convection flows, analytical models such as similarity models, when available, can provide valuable qualitative descriptions of flow behaviour. Such approaches have proved particularly useful in the study of plumes and thermals (Morton, Taylor & Turner 1956; Turner 1962; Fanneløp & Webber 2003; Scase *et al.* 2006; Kaye 2008; Hunt & van den Bremer 2010; Woods 2010) and flows along heated vertical surfaces (Ostrach 1953; Sparrow & Gregg 1958; Ede 1967; Merkin 1985; Gebhart *et al.* 1988). Our present study provides one of the few similarity descriptions of unsteady horizontal free convection flows.

We consider a particularly simple class of horizontal free convection flows schematized in figure 1. Initially quiescent fluid overlies an infinite horizontal boundary placed at $z = 0$. At time $t = 0$, a surface forcing in terms of a negative buoyancy or buoyancy flux is suddenly imposed and thereafter maintained in a steady state. The forcing is spatially constant (piecewise) with a step change at $x = 0$. The thermal boundary layers that arise on either side of the step change develop at different rates, and lateral pressure variations in the transition zone between them drive an intrinsically unsteady, boundary-layer-like flow.

Our study proceeds in a boundary-layer framework, with $x$-derivatives in the viscous stress and diffusion terms neglected, and the hydrostatic approximation invoked. Steady-state versions of these equations were used to study horizontal free convection flows along semi-infinite plates (single edge) (Stewartson 1958, with sign error corrected by Gill, Zeh & del Casal 1965, Rotem & Claassen 1969, Pera & Gebhart 1973, Chen, Tien & Armaly 1986, Deswita *et al.* 2009 and Samanta & Guha 2012), and along finite strips (two edges) (Clifton & Chapman 1969; Singh & Birkebak 1969; Fujii, Honda & Morioka 1973; Dayan, Kushnir & Ullmann 2002; Neufeld, Goldstein & Worster 2010). The single-edge studies considered flows along heated upward-facing surfaces or cooled downward-facing surfaces. Such flows became unstable at some distance from the edge, but exhibited a boundary-layer structure up to the

separation point. The double-edge studies considered flows along heated downward-facing surfaces or cooled upward-facing surfaces. These laterally spreading flows were reminiscent of stagnation point flows.

However, very few analyses have been reported for unsteady horizontal free convection problems. Ingham, Merkin & Pop (1986) considered the response of a heated boundary layer to the sudden cooling of a semi-infinite horizontal upward-facing plate. The initial state satisfied the Stewartson (1958) and Gill *et al.* (1965) similarity model for steady flow along a heated semi-infinite upward facing plate. Higuera (1998) examined the flow induced by the sudden application of a line heat source (singularity at $x = 0$) along an infinite horizontal downward-facing adiabatic surface. Amin & Riley (1990) studied the boundary layer over an infinite horizontal surface whose temperature varied quadratically with $x$ (singularities as $x \to \pm\infty$). A steady state could be achieved if the surface temperature increased away from the plane of symmetry, but if the surface temperature decreased away from the plane of symmetry, the solution became singular throughout the boundary layer at a finite time.

The boundary-layer equations for horizontal free convection flows are presented in § 2. Similarity models for flows of unstratified fluids driven by a step change in surface buoyancy or surface buoyancy flux are obtained by a group-theoretic approach in § 3. A corresponding analysis in § 4 for stratified fluids yields a similarity model only for the flux-forced case. Examples of similarity model predictions are presented in § 5. The predictions are verified using data from numerical simulations in which no boundary-layer approximations are made.

## 2. Governing equations

Consider the two-dimensional flow of a viscous fluid over a horizontal plate (surface) placed at $z = 0$ (figure 1). Within a Boussinesq boundary-layer framework, the governing equations are

$$\frac{\partial u}{\partial t} + u\frac{\partial u}{\partial x} + w\frac{\partial u}{\partial z} = -\frac{\partial \pi}{\partial x} + \nu\frac{\partial^2 u}{\partial z^2}, \tag{2.1}$$

$$0 = -\frac{\partial \pi}{\partial z} + b, \tag{2.2}$$

$$\frac{\partial b}{\partial t} + u\frac{\partial b}{\partial x} + w\frac{\partial b}{\partial z} = -\gamma w + \kappa\frac{\partial^2 b}{\partial z^2}, \tag{2.3}$$

$$\frac{\partial u}{\partial x} + \frac{\partial w}{\partial z} = 0. \tag{2.4}$$

Here $u$ is the lateral ($x$) velocity component; $w$ is the vertical ($z$) velocity component; $\pi \equiv (p - \bar{p})/\rho_r$, where $p$ is pressure, $\bar{p}(z)$ is the pressure in a motionless reference state, and $\rho_r$ is a constant reference density; $b \equiv g\,(\theta - \bar{\theta})/\theta_r$ is buoyancy, where $\theta$ is temperature (of a liquid) or potential temperature (of a gas), $\theta_r$ is a constant reference value of $\theta$, $\bar{\theta}(z)$ is the initial profile of $\theta$, and $g$ is the acceleration due to gravity. The stratification parameter $\gamma \equiv (g/\theta_r)\,\mathrm{d}\bar{\theta}/\mathrm{d}z$, and the coefficients of viscosity $\nu$ and thermal diffusivity $\kappa$ are considered constant.

Taking $\partial/\partial z$ (2.1) $- \partial/\partial x$ (2.2) yields

$$\left(\frac{\partial}{\partial t} + u\frac{\partial}{\partial x} + w\frac{\partial}{\partial z}\right)\frac{\partial u}{\partial z} = -\frac{\partial b}{\partial x} + \nu\frac{\partial^3 u}{\partial z^3}. \tag{2.5}$$

Introducing the streamfunction $\psi$ defined by $u = \partial\psi/\partial z$, $w = -\partial\psi/\partial x$, (2.4) is automatically satisfied, while (2.3) and (2.5) become

$$\left(\frac{\partial}{\partial t} + \frac{\partial\psi}{\partial z}\frac{\partial}{\partial x} - \frac{\partial\psi}{\partial x}\frac{\partial}{\partial z}\right) b = \gamma\frac{\partial\psi}{\partial x} + \kappa\frac{\partial^2 b}{\partial z^2}, \tag{2.6}$$

$$\left(\frac{\partial}{\partial t} + \frac{\partial\psi}{\partial z}\frac{\partial}{\partial x} - \frac{\partial\psi}{\partial x}\frac{\partial}{\partial z}\right)\frac{\partial^2\psi}{\partial z^2} = -\frac{\partial b}{\partial x} + \nu\frac{\partial^4\psi}{\partial z^4}. \tag{2.7}$$

We suppose $b$, $\pi$ and $\partial u/\partial z$ vanish as $z \to \infty$. We do not assume the velocity vanishes as $z \to \infty$ but will look to the solution for its behaviour. The pressure gradient force near the leading edge of an advancing low-level flow will push parcels upward, out of the way of the flow. In an unstratified fluid ($\gamma = 0$), a vertical velocity $-\partial\psi/\partial x = h(x, t) \neq 0$ that persists as $z \to \infty$ (while $b \to 0$) is a solution of (2.6) and (2.7), but in a stratified fluid ($\gamma > 0$), (2.6) shows that if $b \to 0$ as $z \to \infty$ then the vertical velocity also vanishes as $z \to \infty$. This result is not surprising since stratification suppresses vertical motions.

We suppose $\partial b/\partial x$, $u$ and $w$ vanish as $x \to \pm\infty$. In this case all terms in (2.7) vanish, and (2.6) reduces to the diffusion equation, with solutions for a suddenly imposed surface temperature perturbation and surface heat flux given in Carslaw & Jaeger (1959, (10) on p. 60, and (7) on p. 75). In terms of buoyancy, these solutions are, respectively,

$$b(x \to \pm\infty, z, t) = b_0^{\pm}\mathrm{erfc}\left(\frac{z}{2\sqrt{\kappa t}}\right), \tag{2.8}$$

$$b(x \to \pm\infty, z, t) = -2\left.\frac{\mathrm{d}b^{\pm}}{\mathrm{d}z}\right|_{z=0}\left[\sqrt{\frac{\kappa t}{\pi}}\exp\left(-\frac{z^2}{4\kappa t}\right) - \frac{z}{2}\mathrm{erfc}\left(\frac{z}{2\sqrt{\kappa t}}\right)\right], \tag{2.9}$$

where a superscript $\pm$ denotes $x \to \pm\infty$. Equation (2.9) shows that the surface buoyancy in the flux-forced case varies as $t^{1/2}$. In both cases the depth of the disturbance increases with time.

We solve (2.6) and (2.7) subject to remote ($z \to \infty$) conditions of vanishing $\partial u/\partial z$ and $b$, surface conditions of no-slip, impermeability, and specified $b$ or $\partial b/\partial z$, and the condition that results from evaluating (2.1) at $z = 0$, with the surface $\pi$ obtained from integration of (2.2),

$$\left.\frac{\partial^2 u}{\partial z^2}\right|_{z=0} = -\frac{1}{\nu}\frac{\partial}{\partial x}\int_0^{\infty} b\,\mathrm{d}z. \tag{2.10}$$

We non-dimensionalize variables with an eye on minimizing the number of free parameters. A buoyancy scale $b_s > 0$ is defined in terms of a surface buoyancy or surface buoyancy flux as

$$b_s \equiv \max|b|_{z=0} \qquad \text{(prescribed surface buoyancy)}, \tag{2.11}$$

$$b_s \equiv \max \kappa^{1/2}\,(\mathrm{d}b/\mathrm{d}z|_{z=0})^{3/4} \qquad \text{(prescribed surface buoyancy flux)}. \tag{2.12}$$

In terms of the non-dimensional variables,

$$X \equiv b_s^{1/3}x/\nu^{2/3}, \quad Z \equiv b_s^{1/3}z/\nu^{2/3}, \quad T \equiv b_s^{2/3}t/\nu^{1/3}, \quad B \equiv b/b_s, \quad \Psi \equiv \psi/\nu, \tag{2.13}$$

equations (2.6) and (2.7) become

$$\left(\frac{\partial}{\partial T}+\frac{\partial \Psi}{\partial Z}\frac{\partial}{\partial X}-\frac{\partial \Psi}{\partial X}\frac{\partial}{\partial Z}\right)B=\Gamma\frac{\partial \Psi}{\partial X}+\frac{1}{Pr}\frac{\partial^2 B}{\partial Z^2}, \tag{2.14}$$

$$\left(\frac{\partial}{\partial T}+\frac{\partial \Psi}{\partial Z}\frac{\partial}{\partial X}-\frac{\partial \Psi}{\partial X}\frac{\partial}{\partial Z}\right)\frac{\partial^2 \Psi}{\partial Z^2}=-\frac{\partial B}{\partial X}+\frac{\partial^4 \Psi}{\partial Z^4}, \tag{2.15}$$

where $Pr\equiv \nu/\kappa$ is the Prandtl number and $\Gamma\equiv \gamma\,\nu^{2/3}b_s^{-4/3}$ is a stratification parameter.

With the larger forcing put to the left of the step change, (2.11) and (2.12) become

$$B(X,0,T)=\begin{cases}-1, & X\leqslant 0,\\ -\varepsilon, & X>0,\end{cases} \tag{2.16}$$

$$\left.\frac{\partial B}{\partial Z}\right|_{Z=0}=\begin{cases}Pr^{2/3}, & X\leqslant 0,\\ \varepsilon Pr^{2/3}, & X>0,\end{cases} \tag{2.17}$$

where $\varepsilon$ $(0\leqslant\varepsilon\leqslant 1)$ is a reduction factor. The remaining conditions become

$$\Psi(X,0,T)=0,\quad \left.\frac{\partial \Psi}{\partial Z}\right|_{Z=0}=0,\quad \left.\frac{\partial^3 \Psi}{\partial Z^3}\right|_{Z=0}=-\frac{\partial}{\partial X}\int_0^\infty B\,\mathrm{d}Z, \tag{2.18}$$

$$\frac{\partial^2 \Psi}{\partial Z^2},\ B\to 0\quad \text{as } Z\to\infty, \tag{2.19}$$

$$\frac{\partial^2 \Psi}{\partial Z^2}(X,Z,0)=0,\quad B(X,Z,0)=0,\quad (Z>0). \tag{2.20}$$

Only three parameters appear in the non-dimensional problem: $Pr$, $\Gamma$ and $\varepsilon$.

## 3. Similarity model for the unstratified fluid case ($\Gamma=0$)

We use a group-theoretic approach (e.g. Bluman & Cole 1974; Dresner 1983, 1999; Barenblatt 1996) to obtain similarity solutions of (2.14) and (2.15). Our focus on step changes in the buoyancy and buoyancy flux is motivated by the fortuitous outcome of the group analyses.

### 3.1. *Invariance to the stretching transformation*

Consider the one-parameter group of stretching transformations

$$T'=\mu\,T,\quad X'=\mu^m X,\quad Z'=\mu^q Z,\quad \Psi'=\mu^r\Psi,\quad B'=\mu^s B, \tag{3.1}$$

where $\mu$ is a continuous parameter and $\mu=1$ is the identity element. Equations (2.14) and (2.15) with $\Gamma=0$ are invariant to (3.1) provided $m=r+1/2$, $q=1/2$, $s=2r-3/2$, where $r$ is arbitrary. Equation (3.1) maps any solution $B=g(X,Z,T)$, $\Psi=f(X,Z,T)$ of (2.14) and (2.15) to another solution of (2.14) and (2.15). We consider special cases for which the solutions themselves are invariant to (3.1), that is, $\mu^s g(X,Z,T)=g(\mu^m X,\mu^q Z,\mu T)$ and $\mu^r f(X,Z,T)=f(\mu^m X,\mu^q Z,\mu T)$. Differentiating these equations with respect to $\mu$, and setting $\mu=1$, yields partial differential equations for $g$ and $f$ whose general solutions yield

$$\Psi=T^{-\sigma-1/2}F(\xi,\eta),\quad B=T^{-2\sigma-5/2}G(\xi,\eta), \tag{3.2}$$

$$\xi\equiv XT^{\sigma},\quad \eta\equiv ZT^{-1/2}, \tag{3.3}$$

where $\sigma \equiv -r - 1/2$. In view of (3.2) and (3.3), (2.14) and (2.15) reduce to

$$\left(-2\sigma - \frac{5}{2} + \sigma\xi\frac{\partial}{\partial\xi} - \frac{1}{2}\eta\frac{\partial}{\partial\eta} + \frac{\partial F}{\partial\eta}\frac{\partial}{\partial\xi} - \frac{\partial F}{\partial\xi}\frac{\partial}{\partial\eta}\right) G = \frac{1}{Pr}\frac{\partial^2 G}{\partial\eta^2}, \tag{3.4}$$

$$\left(-\sigma - \frac{3}{2} + \sigma\xi\frac{\partial}{\partial\xi} - \frac{1}{2}\eta\frac{\partial}{\partial\eta} + \frac{\partial F}{\partial\eta}\frac{\partial}{\partial\xi} - \frac{\partial F}{\partial\xi}\frac{\partial}{\partial\eta}\right)\frac{\partial^2 F}{\partial\eta^2} = -\frac{\partial G}{\partial\xi} + \frac{\partial^4 F}{\partial\eta^4}, \tag{3.5}$$

while the surface conditions (2.18) become

$$F(\xi, 0) = 0, \quad \left.\frac{\partial F}{\partial\eta}\right|_{\eta=0} = 0, \quad \left.\frac{\partial^3 F}{\partial\eta^3}\right|_{\eta=0} = -\frac{\partial}{\partial\xi}\int_0^\infty G\,\mathrm{d}\eta, \tag{3.6}$$

and the remote conditions (2.19) and the initial conditions (2.20) conflate to

$$\frac{\partial^2 F}{\partial\eta^2}, G \to 0 \quad \text{as } \eta \to \infty. \tag{3.7}$$

We next identify values of $\sigma$ that yield surface forcings that satisfy (2.16) or (2.17).

### 3.2. *Step change in surface buoyancy*

For $B(X, 0, T) = T^{-2\sigma-5/2}G(\xi, 0)$ to be in a steady state, the time dependence implicit in $G(\xi, 0)$ must cancel the $T^{-2\sigma-5/2}$ factor. This constrains $G(\xi, 0)$ to the form $C\xi^{2+5/(2\sigma)}$ (so $B(X, 0, T) = CX^{2+5/(2\sigma)}$), where $C$ is constant or piecewise constant with a step change at $X = 0$. Thus, for (2.16) to be satisfied, $C$ is piecewise constant and $\sigma$ is $-5/4$. In this case,

$$G(\xi, 0) = \begin{cases} -1, & \xi \leqslant 0, \\ -\varepsilon, & \xi > 0, \end{cases} \tag{3.8}$$

while (3.2) and (3.3) become

$$\Psi = T^{3/4}F(\xi, \eta), \quad B = G(\xi, \eta), \tag{3.9}$$

$$\xi \equiv XT^{-5/4}, \quad \eta \equiv ZT^{-1/2}. \tag{3.10}$$

The dimensional variables corresponding to this flow are

$$u = \nu^{1/4}b_s^{1/2}t^{1/4}\frac{\partial F}{\partial\eta}, \quad w = -\nu^{1/2}t^{-1/2}\frac{\partial F}{\partial\xi}, \quad b = b_s G. \tag{3.11}$$

From (3.11) we see that local extrema in $u$ are located at points $\xi = \xi_c$, $\eta = \eta_c$ satisfying $\partial^2 F/\partial\eta^2 = \partial^2 F/\partial\xi\,\partial\eta = 0$, and thus propagate along trajectories given by

$$\frac{\mathrm{d}X}{\mathrm{d}T} = \frac{5}{4}\xi_c T^{1/4}, \quad (X = \xi_c T^{5/4}), \quad \frac{\mathrm{d}Z}{\mathrm{d}T} = \frac{1}{2}\eta_c T^{-1/2}, \quad (Z = \eta_c T^{1/2}). \tag{3.12}$$

More generally, the trajectory of any extremum of any order of $u$, $w$, or $b$ satisfies (3.12). Since $Z \propto T^{1/2}$ and $X \propto T^{5/4}$, the extrema radiate outward on paths $Z \propto X^{2/5}$ (except for paths along the $Z$-axis). Since the lateral spread $\Delta X$ between any two extrema not on the $Z$-axis varies as $\Delta X \propto T^{5/4}$, while the vertical spread $\Delta Z$ varies as $\Delta Z \propto T^{1/2}$, the lag of any extremum of any variable behind any other extremum increases with time.

It can also be noted from (3.9) that $B$ is itself constant along curves defined by constant values of $\xi$ and $\eta$. Thus, the $B$ field propagates according to (3.12).

Since $\xi$ and $\eta$ are constant along the trajectories of the extrema, (3.9)–(3.11) and (2.13) can be used to deduce the evolution of the amplitudes of these extrema. We obtain, for example,

$$u_{max} \propto \nu^{1/4} b_s^{1/2} t^{1/4}, \quad w_{max} \propto \nu^{1/2} t^{-1/2}, \tag{3.13a}$$

$$\partial u/\partial z_{max} \propto \nu^{-1/4} b_s^{1/2} t^{-1/4}, \quad \partial u/\partial x_{max} \propto t^{-1}, \quad \partial b/\partial z_{max} \propto \nu^{-1/2} b_s t^{-1/2}. \tag{3.13b}$$

### 3.3. *Step change in surface buoyancy flux*

For $\partial B/\partial Z|_{Z=0} = T^{-2\sigma-3}\partial G/\partial\eta|_{\eta=0}$ to be in a steady state, the time dependence in $\partial G/\partial\eta|_{\eta=0}$ must cancel the $T^{-2\sigma-3}$ factor. In view of (3.2) and (3.3), this can only happen if $\partial G/\partial\eta|_{\eta=0} = D\xi^{2+3/\sigma}[\partial B/\partial Z|_{Z=0} = DX^{2+3/\sigma}]$, where $D$ is constant or piecewise constant. Thus, for (2.17) to be satisfied, $D$ is piecewise constant and $\sigma$ is $-3/2$. In this case,

$$\left.\frac{\partial G}{\partial\eta}\right|_{\eta=0} = \begin{cases} Pr^{2/3}, & \xi \leqslant 0, \\ \varepsilon Pr^{2/3}, & \xi > 0, \end{cases} \tag{3.14}$$

while (3.2) and (3.3) become

$$\Psi = TF(\xi,\eta), \quad B = T^{1/2}G(\xi,\eta), \tag{3.15}$$

$$\xi \equiv XT^{-3/2}, \quad \eta \equiv ZT^{-1/2}. \tag{3.16}$$

The corresponding dimensional variables are

$$u = b_s^{2/3}\nu^{1/6}t^{1/2}\frac{\partial F}{\partial\eta}, \quad w = -\nu^{1/2}t^{-1/2}\frac{\partial F}{\partial\xi}, \quad b = \frac{b_s^{4/3}t^{1/2}}{\nu^{1/6}}G. \tag{3.17}$$

These scalings yield the speeds and trajectories of all local extrema of $u$, $w$ and $b$ of any order:

$$\frac{\mathrm{d}X}{\mathrm{d}T} = \frac{3}{2}\xi_c T^{1/2}, \quad (X = \xi_c T^{3/2}), \quad \frac{\mathrm{d}Z}{\mathrm{d}T} = \frac{1}{2}\eta_c T^{-1/2}, \quad (Z = \eta_c T^{1/2}), \tag{3.18}$$

where $\xi_c$ and $\eta_c$ identify a particular extremum. Since $Z \propto T^{1/2}$ and $X \propto T^{3/2}$, the extrema travel along paths $Z \propto X^{1/3}$ (except for paths along the $Z$-axis). The spread between any two local extrema not on the $Z$-axis varies according to $\Delta X \propto T^{3/2}$ and $\Delta Z \propto T^{1/2}$.

Equation (3.17) also shows that the vorticity $\partial^2\Psi/\partial Z^2$ and $\partial B/\partial Z$ are themselves constant on curves for which $\xi$ and $\eta$ are constant. Thus, these patterns also propagate according to (3.18).

The similarity scalings again reveal the evolution of the amplitudes of the local extrema. Using (3.17) together with (3.15), (3.16) and (2.13), we find that

$$u_{max} \propto b_s^{2/3}\nu^{1/6}t^{1/2}, \quad w_{max} \propto \nu^{1/2}t^{-1/2}, \tag{3.19a}$$

$$\partial u/\partial z_{max} \propto \nu^{-1/3}b_s^{2/3}, \quad \partial u/\partial x_{max} \propto t^{-1}, \quad \partial b/\partial z_{max} \propto \nu^{-2/3}b_s^{4/3}. \tag{3.19b}$$

## 4. Similarity model for the stably stratified fluid case ($\Gamma > 0$)

For a stably stratified fluid ($\Gamma > 0$), we find that (2.14) and (2.15) are invariant to (3.1) provided $q = 1/2$, $m = 3/2$, $s = 1/2$, $r = 1 (\sigma = -3/2)$. There is no arbitrary exponent as there was in § 3.1 for the case of an unstratified fluid. Thus, (3.2) and (3.3) become

$$\Psi = TF(\xi,\eta), \quad B = T^{1/2}G(\xi,\eta), \tag{4.1}$$

$$\xi \equiv XT^{-3/2}, \quad \eta \equiv ZT^{-1/2}, \tag{4.2}$$

which are identical to (3.15) and (3.16) for a step change in the surface buoyancy flux in an unstratified fluid. Thus, the only acceptable surface thermal boundary condition in this case is the flux condition (3.14).

Since (4.1) and (4.2) are identical to (3.15) and (3.16), the propagation of any local extremum of $u$, $w$ and $b$ of any order is again described by (3.18), and the amplitudes of selected extrema satisfy (3.19). Again we see that the lateral spread between any two local extrema that are not on the $Z$-axis varies as $\Delta X \propto T^{3/2}$, while the vertical spread varies as $\Delta Z \propto T^{1/2}$.

## 5. Examples

Similarity model predictions are presented for flows of unstratified fluids ($\Gamma = 0$) forced by a step change in surface buoyancy (case UB) and buoyancy flux (case UF), and flows of stratified fluids (with $\Gamma = 0.5$) forced by a step change in surface buoyancy flux (case SF) – all with default settings of $\varepsilon = 0.5$ and $Pr = 1$. Results are then shown for other values of $\varepsilon$ and $Pr$. Predictions are verified using data from numerical solutions of governing equations in which no boundary-layer approximations are made.

### 5.1. *Generation of verification data by numerical simulation*

Verification data are obtained by solving the Boussinesq equations of motion, the thermal energy equation, and the elliptic equation for $\pi$ that results from taking the divergence of the equations of motion. No boundary-layer approximations are made in those equations. The numerical procedures are similar to those used in Fedorovich & Shapiro (2009*a*,*b*). The computer code was originally designed for three-dimensional simulation, but was adapted for use in a two-dimensional mode: to simulate a laminar flow that is independent of $y$, one allocates four grid points in the $y$ direction and imposes periodicity in that direction.

The model equations are discretized on a staggered Cartesian grid with uniform grid spacing. The prognostic variables are integrated using a leapfrog scheme. The equation for $\pi$ is solved using a fast Fourier transform technique over horizontal planes, and a tridiagonal matrix inversion in the $z$ direction, with $\partial\pi/\partial z$ at the surface calculated as a residual from the vertical equation of motion. At the domain top, the vertical gradients of all variables are set to zero. Periodic conditions are imposed on the lateral boundaries.

Although periodicity in $x$ is not strictly consistent with flow driven by a single step change, such flows can be emulated in a periodic framework with a top-hat forcing (two anti-symmetric step changes) provided the steps are far from each other and the $x$-boundaries. After a sufficiently long time, however, flows arising from the steps will interact. A top-hat simulation can only serve as a proxy for a single step change flow prior to the onset of that interaction.

With the top-hat forcing centred on the mid-point of the computational domain and extending across half the domain, we need only consider results in the right half of the domain. The origin $x = 0$, $z = 0$ coincides with the step change in that part of the domain. Case UB is run with

$$b(x, 0, t) = \begin{cases} -0.2 \text{ m s}^{-2}, & x \leqslant 0, \\ -0.1 \text{ m s}^{-2}, & x > 0, \end{cases} \tag{5.1}$$

while UF and SF are run with

$$\left.\frac{\partial b}{\partial z}\right|_{z=0} = \begin{cases} 0.002 \text{ s}^{-2}, & x \leqslant 0, \\ 0.001 \text{ s}^{-2}, & x > 0. \end{cases} \tag{5.2}$$

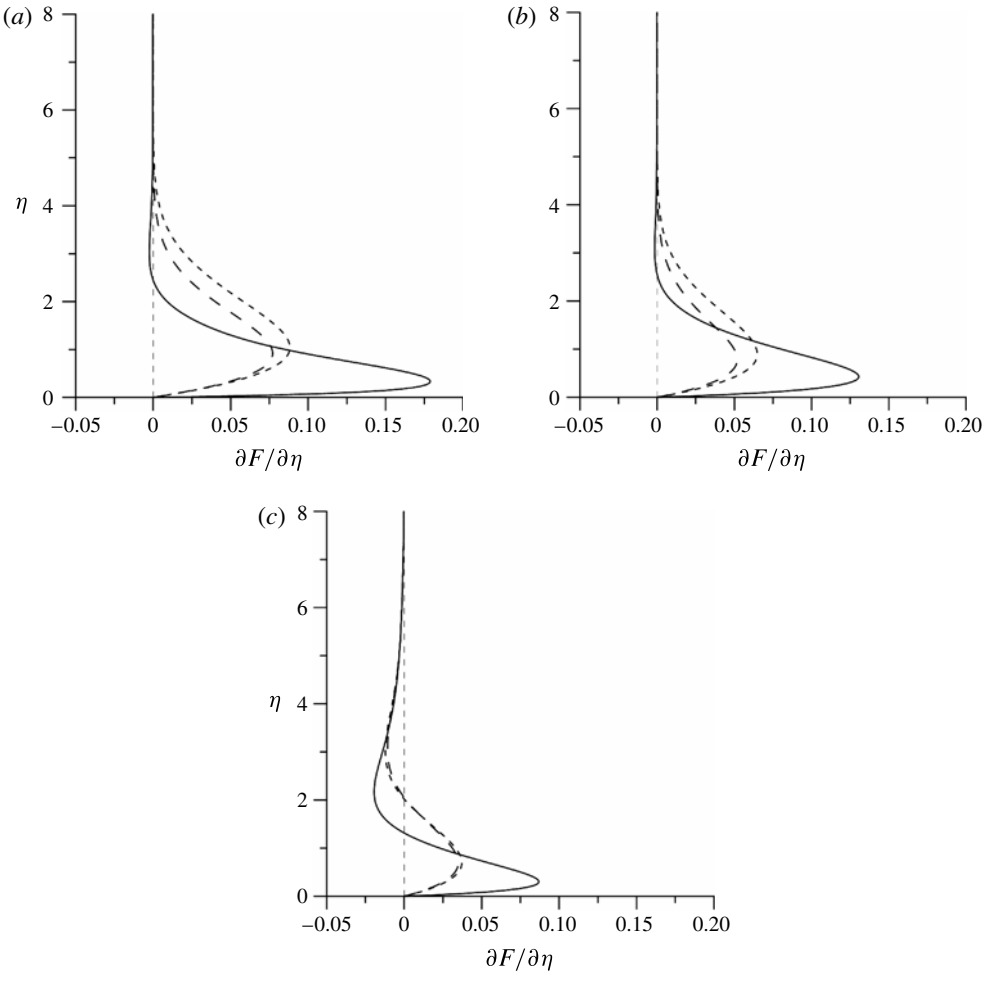


FIGURE 2. Non-dimensional profiles of the horizontal velocity function $\partial F/\partial\eta$ for cases UB (*a*), UF (*b*), and SF (*c*). Profiles are shown at $\xi = -0.2$ (long-dashed line), $\xi = 0$ (solid line), and $\xi = 0.2$ (short-dashed line).

The domain is 8192 m long and 800 m tall, the grid spacing is $\Delta x = \Delta z = 1$ m, $\gamma$ is zero in UB and UF, and 0.001 $\mathrm{s}^{-2}$ in SF, and the default values of $\nu$ and $\kappa$ are 1 $\mathrm{m}^2\ \mathrm{s}^{-1}$.

### 5.2. *Similarity model solution*

Pseudo-time-derivative terms are introduced into (3.4) and (3.5), which are integrated (iterated) on an unstaggered Cartesian ($\xi$, $\eta$) grid using a leapfrog scheme. During each iteration, (3.5) is solved for a vorticity function $\mu(\equiv\partial^2 F/\partial\eta^2)$, and $F$ is diagnosed from the recursion relation $F_{k+1} = 2F_k - F_{k-1} + \mu_k(\Delta\eta)^2$ obtained from $\partial^2 F/\partial\eta^2 = \mu$ ($\Delta\eta$ is the grid spacing of the $\eta$ coordinate, $k$ is the $\eta$-grid index). With the lowest two grid points straddling the surface, the no-slip and impermeability conditions yield $F_1 = F_2 = 0$. Those values are used to start the upward sweep of the recursion relation. The procedure is deemed to have converged when $G$ and $\mu$ barely change between iterations.

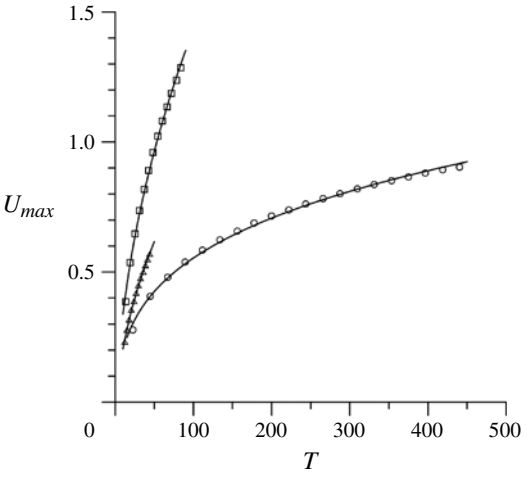


FIGURE 3. Evolution of maximum horizontal velocity component $U_{max}$ from numerical simulations of cases UB (circles), UF (squares), and SF (triangles). Solid lines depict the corresponding two-parameter fits of the similarity power laws for $U_{max}$: $0.256\,T^{1/4} - 0.255$ (case UB), $0.160\,T^{1/2} - 0.168$ (case UF), and $0.105\,T^{1/2} - 0.128$ (case SF).

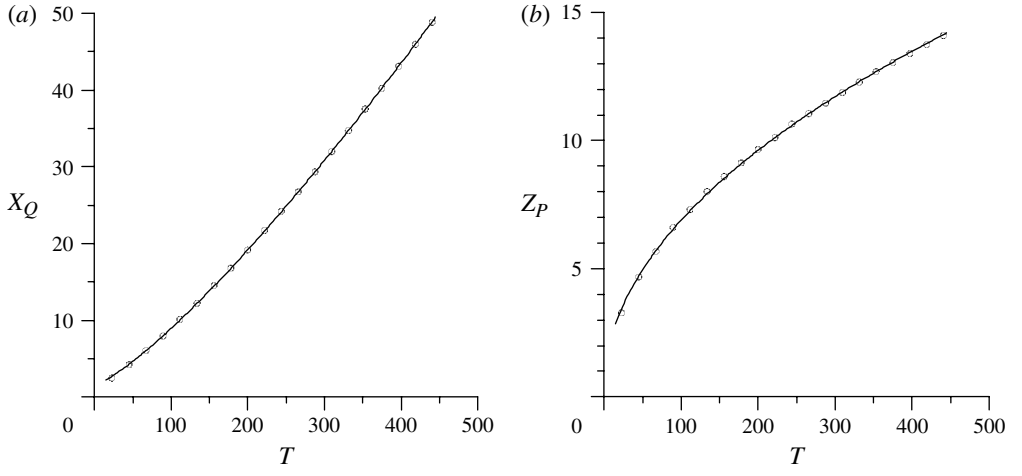


FIGURE 4. Trajectories of two selected points on a buoyancy isoline ($B = -0.5$) from case UB; (*a*) $X_Q$, $X$-component of trajectory of point $Q$ as it moves along (slightly above) the surface, and (*b*) $Z_P$, $Z$-component of trajectory of point $P$ as it moves along the vertical axis. Numerical simulation results are indicated by circles. Solid lines are the corresponding two-parameter fits of the similarity power laws: $X_Q = 0.0234T^{5/4} + 1.51$, $Z_P = 0.655T^{1/2} + 0.293$.

Equations (3.4) and (3.5) are solved subject to (3.6) and (3.7), and either (3.8) (for UB) or (3.14) (for UF and SF) with $Pr = 1$ and $\varepsilon = 0.5$. The stratification parameter $\Gamma$ is set to zero in UB and UF, and to 0.5 in SF (consistent with values of $\nu$, $\kappa$, $\gamma$, and buoyancy flux used to generate the SF verification data). The computational grid $\eta \in [0, 12]$, $\xi \in [-1.5, 1.5]$, is discretized with a spacing of $\Delta\eta = 0.01$, $\Delta\xi = 0.001$. Preliminary tests were hampered by build-up of $2\Delta\xi$ noise that led to instability. This

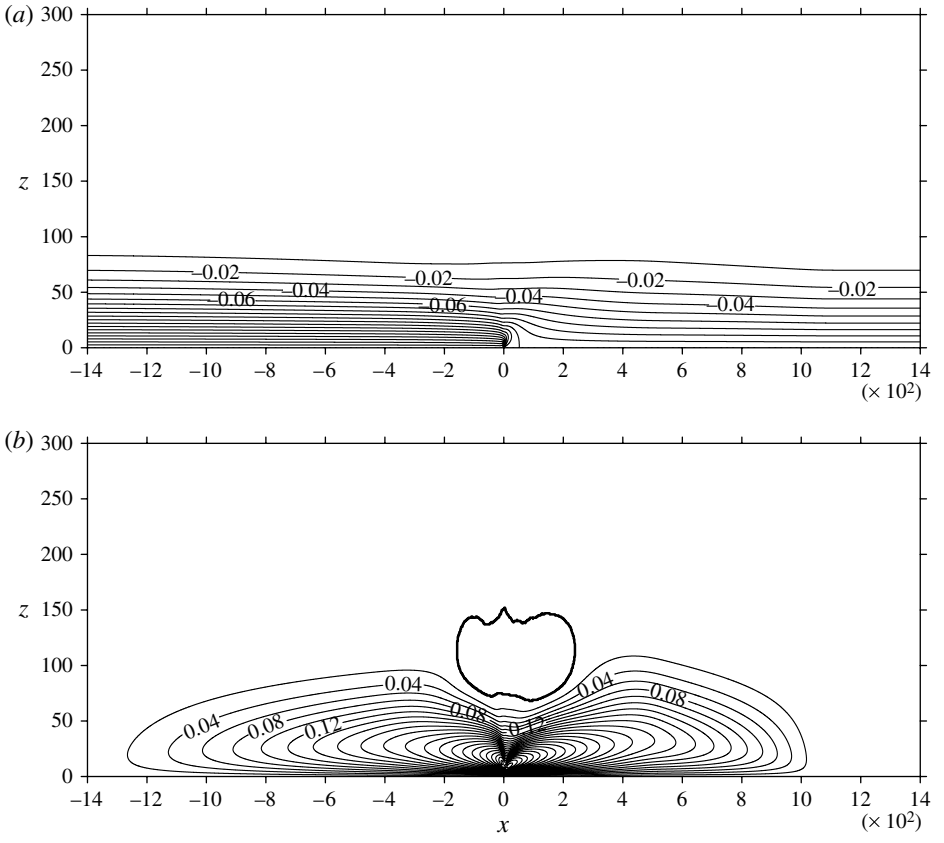


FIGURE 5. Vertical cross-sections of $b$ ($a$; in m s$^{-2}$) and $u$ ($b$; in m s$^{-1}$) in case UB from the similarity model at $t = 905$ s. The thick line marks the zero contour for $u$. Coordinates are in metres.

noise was suppressed by applying a fourth-order filter (Skamarock 2004; Jablonowski & Williamson 2011) in the $\xi$ direction in (3.4) and (3.5). The results shown here were obtained with a filter constant large enough to mitigate the noise but small enough that the main features of interest are relatively unaffected.

### 5.3. *Results*

Non-dimensional vertical profiles of the similarity-model predicted horizontal velocity function $\partial F/\partial\eta$ for cases UB, UF and SF are shown in figure 2. The flows are shallow and jet-like, with peak winds found close to the step change ($\xi = 0$). The flows are primarily directed from the colder region to the less cold region, as would be expected for a hydrostatic forcing mechanism. The profiles at $\xi = -0.2$ and $\xi = 0.2$ show that the flows in UB and UF are slightly asymmetric, with the downstream flow stronger than the upstream flow. In contrast, the flow in SF is much more symmetric about the step change. Figure 2 also reveals a notable return flow ($\partial F/\partial\eta < 0$) atop the primary flow in SF. The return flows in UB and UF are barely discernible.

Very good agreement between the evolution of $u_{max}$ from the similarity theory ((3.13) for UB; (3.19) for UF and SF) and from the numerical simulations (both rendered non-dimensional) is seen in figure 3. The validity of (3.12) for the

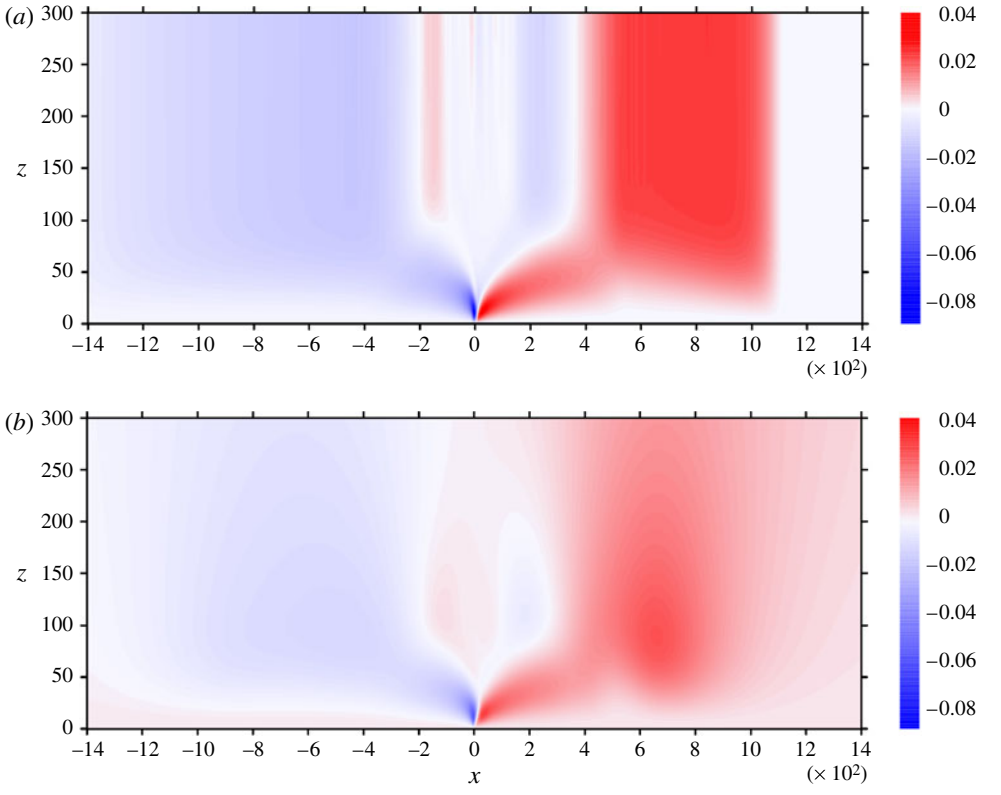


FIGURE 6. Vertical cross-sections of $w$ (in m s$^{-1}$) in case UB from the similarity model ($a$) and from numerical simulation ($b$) at $t = 905$ s. Coordinates are in metres.

propagation of the buoyancy field in UB is confirmed by tracking the trajectories of two points on a $B$ isoline (figure 4). Point $P$ on the $Z$-axis is predicted to stay on that axis and increase its height as $T^{1/2}$. Point $Q$, located just slightly above the surface, is predicted to barely change its height but to be displaced laterally as $T^{5/4}$. The similarity-model predicted trajectories agree well with those from the numerical simulation. Note, however, that the power law fits in these figures include offset factors accounting for the early period in the numerical simulations during which the boundary-layer-like nature of the flow was becoming established.

Vertical cross-sections of the similarity-model predicted $b$, $u$ and $w$ fields for case UB at $t = 905$ s are shown in figures 5 and 6. Here, and in the other cases, the similarity solutions are converted to dimensional form to facilitate comparisons with the numerically simulated (verification) data. The transition of buoyancy between the two diffusing background states occurs over a small distance in the vicinity of the step change. A much broader pattern is seen in the $u$ field. The flow has a boundary-layer character, with the peak $u$ being an order of magnitude larger than the peak $w$. Despite the advection of buoyancy by the primary flow, the close association of the peak horizontal buoyancy gradient with the step change indicates that diffusion of buoyancy from the underlying surface dominates the buoyancy-field structure. In this sense, the flow differs from the more intense gravity currents in nature, where a well-mixed layer of dense fluid intruding into a less dense environment is associated with sharp

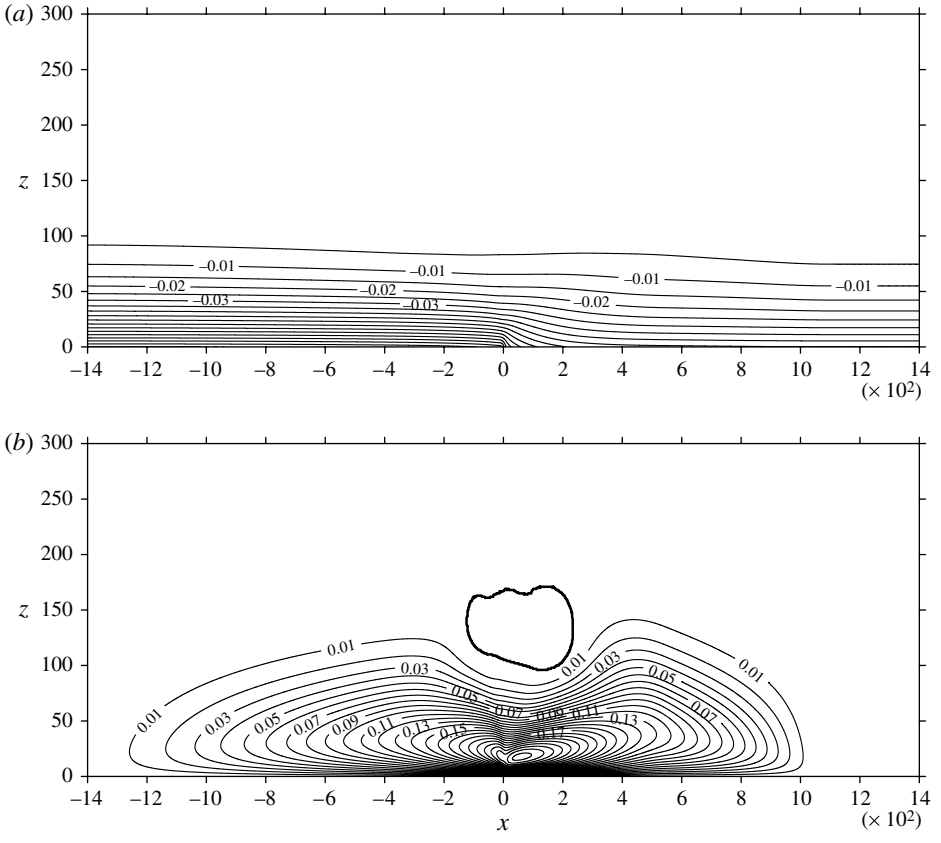


FIGURE 7. Vertical cross-sections of $b$ ($a$; in m s$^{-2}$) and $u$ ($b$; in m s$^{-1}$) in case UF from the similarity model at $t = 1612$ s. The thick line marks the zero contour for $u$. Coordinates are in metres.

horizontal contrasts in momentum and buoyancy in a narrow propagating frontal zone (Simpson 1987).

Good agreement is found between the similarity-model predicted and numerically simulated $b$ and $u$ fields (figures not shown). In particular, the peak $u$ in the numerical simulation ($u_{max} \simeq 0.48$ m s$^{-1}$) is nearly the same as in the similarity prediction ($u_{max} \simeq 0.49$ m s$^{-1}$). The strength of the return flow in the numerical simulation, though very weak, is slightly stronger than in the similarity prediction ($u_{min} \simeq -0.020$ m s$^{-1}$ versus $u_{min} \simeq -0.013$ m s$^{-1}$). Although more significant discrepancies appear between the similarity-model predicted and numerically simulated $w$ fields (figure 6), the small-scale downdraft/updraft couplet in the vicinity of the step change, the broad zones of subsidence upstream of $\xi = 0$ and of ascent downstream of $\xi = 0$, as well as the relative weakness of $w$ are similar. The similarity-model predicted $w$ shows no tendency to vanish far above the surface (recall the discussion in § 2 of the possible behaviour of $w$ as $z \to \infty$). In the numerical simulation, $w$ does decrease with height, but the decrease is gradual, and the $w$ disturbance extends far above the thermal and momentum boundary layers. Thus, the similarity model at least qualitatively captures the main features of the vertical motion.

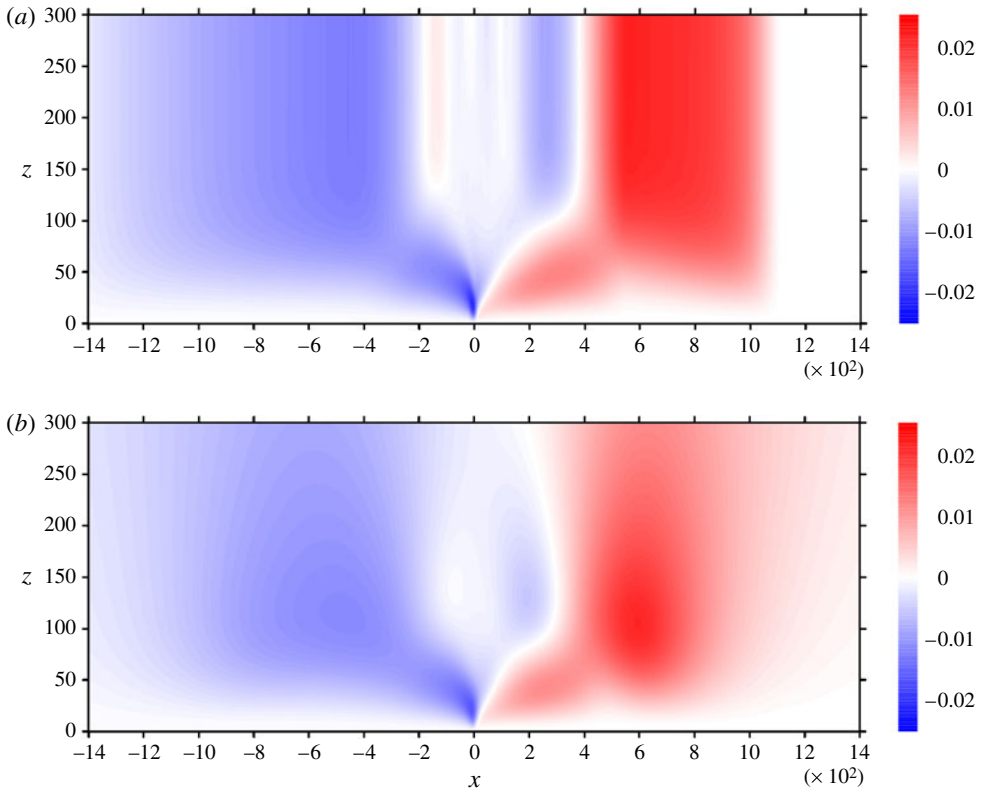


FIGURE 8. Vertical cross-sections of $w$ (in m s$^{-1}$) in case UF from the similarity model ($a$) and from numerical simulation ($b$) at $t = 1612$ s. Coordinates are in metres.

Cross-sections of the $b$, $u$ and $w$ fields for case UF at $t = 1612$ s are shown in figures 7 and 8. The main flow features evident in UB are also seen in UF: the narrow transition zone in the $b$ field, the broad primary flow, the weak return flow atop the primary flow, the downdraft/updraft couplet in the vicinity of the step change, and the tendency for the $w$ disturbance to extend well above the thermal and momentum boundary layers. There is good agreement between the similarity predicted and numerically simulated $b$ and $u$ fields. The peak velocity is $u_{max} \simeq 0.25$ m s$^{-1}$ from both approaches. The (very weak) return flow strength is $u_{min} \simeq -0.015$ m s$^{-1}$ in the numerical simulation and $u_{min} \simeq -0.005$ m s$^{-1}$ in the similarity prediction.

Cross-sections of the $b$, $u$ and $w$ fields for case SF at $t = 994$ s are shown in figures 9 and 10. An updraft/downdraft couplet is still found near $\xi = 0$, but the broad zones of subsidence and ascent extending far above the boundary layer in UB and UF are now almost entirely absent as stratification has suppressed the vertical motion. Compared to UF, the primary flow in SF is much weaker and the return flow is much stronger. The ratio of return flow to primary flow intensities in SF has increased to $\sim$25 %. Since the peak primary and return flows in each similarity model evolve according to the same power laws, that is, (3.13) for UB and (3.19) for UF and SF, their ratio is independent of time. In the SF case there is not only good agreement between the similarity-model predicted and numerically simulated $b$ and $u$ fields (figures not shown), but also between the $w$ fields (figure 10).

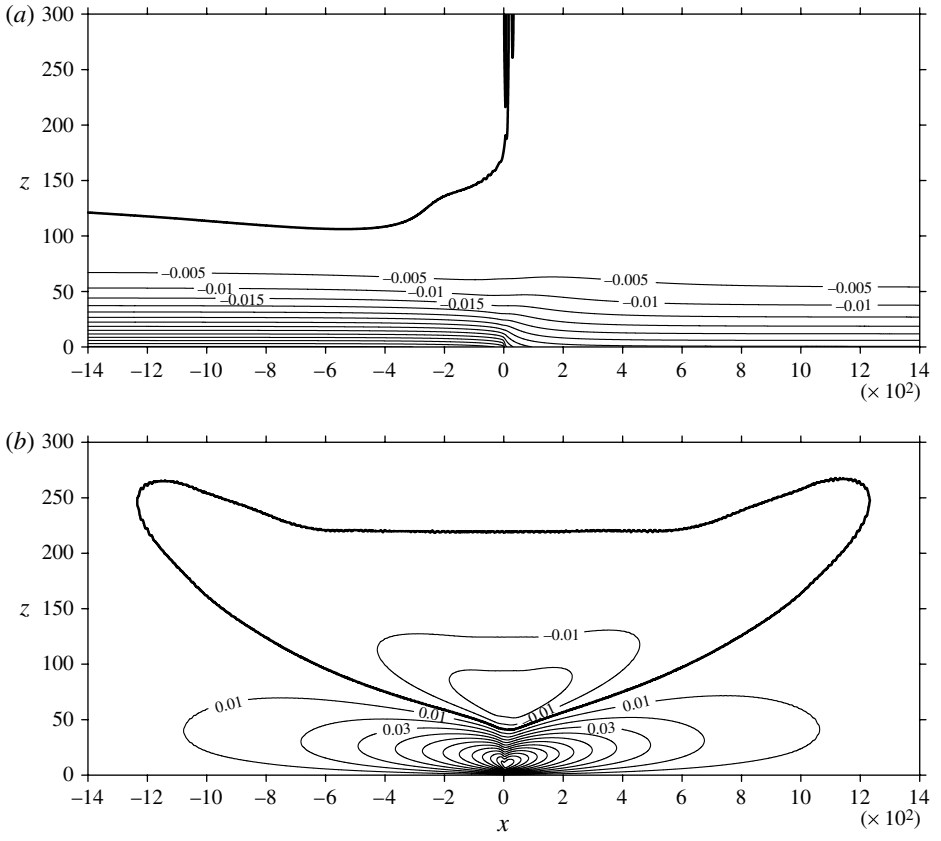


FIGURE 9. Vertical cross-sections of $b$ ($a$; in m s$^{-2}$) and $u$ ($b$; in m s$^{-1}$) in case SF from the similarity model at $t = 994$ s. Thick lines mark zero contours for $b$ and $u$. Coordinates are in metres.

The values of the peak $u$ and return flow velocity from the numerical simulation ($u_{max} \simeq 0.12$ m s$^{-1}$, $u_{min} \simeq -0.030$ m s$^{-1}$) are very close to those from the similarity prediction ($u_{max} \simeq 0.13$ m s$^{-1}$, $u_{min} \simeq -0.028$ m s$^{-1}$). Small-amplitude vertical streaks evident in the similarity solution for $w$ are a computational artefact (see § 5.2).

We next examine the sensitivity of the flow to changes in the reduction parameter $\varepsilon$ with $Pr = 1$. The similarity solutions for the maximum primary flow velocity and the height of the maximum are shown for $\varepsilon = 0.75, 0.5, 0.25$ in figure 11. Apart from being characterized by more peaked maximum velocity curves, the results for UB are qualitatively similar to those for UF: the primary flow becomes stronger and more asymmetric as $\varepsilon$ decreases. The leading edges of the flows in the $\varepsilon = 0.25$ cases are steeper and more front-like than in the larger $\varepsilon$ cases. Although the zones of largest horizontal buoyancy gradient (not shown) are displaced slightly more downstream in the $\varepsilon = 0.25$ cases, they are still close to the step change and thus notably lag the momentum fronts. One can also note that the maximum velocity curves exhibit a peculiar zigzag near $\xi = 0$, most noticeably in case UB. That feature arises from a subtle two-lobe structure in the $u$ field near $x = 0$ (evident in close-up plots, not shown). The maximum velocity in the stratified fluid case SF also increases with a decrease in $\varepsilon$. However, unlike UB and UF, there is little tendency for the SF flow to

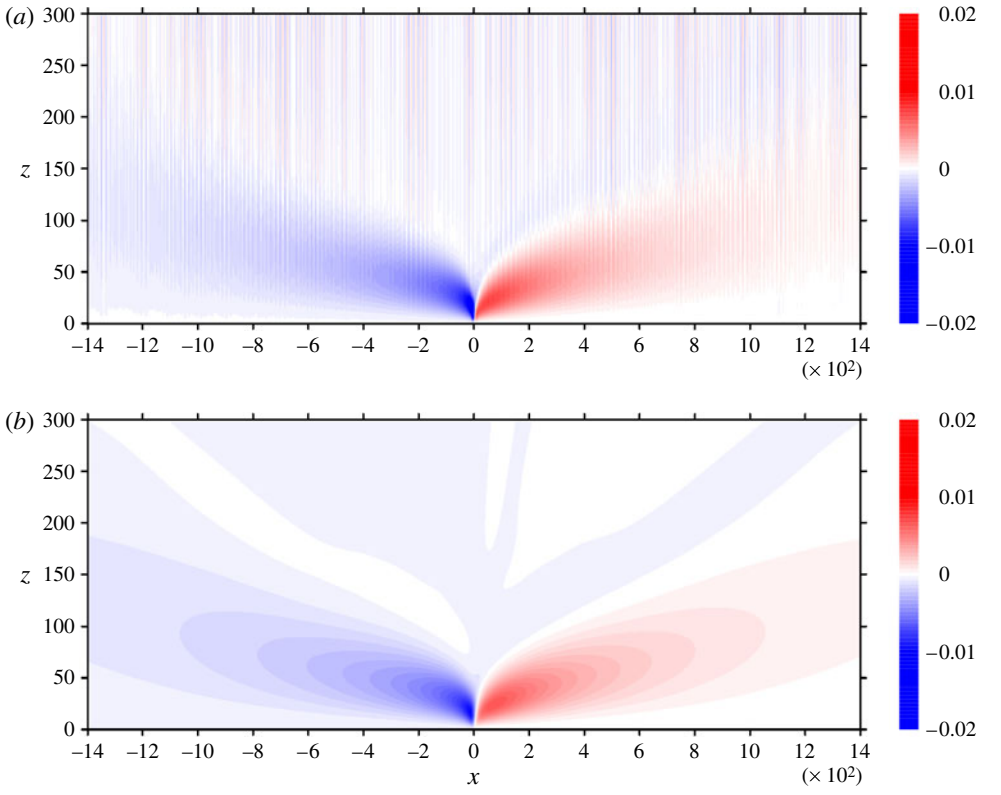


FIGURE 10. Vertical cross-sections of $w$ (in m s$^{-1}$) in case SF from the similarity model ($a$) and from numerical simulation ($b$) at $t = 994$ s. Coordinates are in metres.

become front-like or develop a significant flow asymmetry as $\varepsilon$ decreases. Of the two flux-forced cases, the flow in UF is significantly stronger than in SF, regardless of $\varepsilon$.

Lastly, we illustrate the $Pr$-dependence of the flow in the UB case, with $\varepsilon = 0.5$. In the numerical simulations, $Pr$ was varied by changing $\kappa$, with $\nu$ fixed. By considering $\nu$ fixed in the similarity model, (2.11) and (2.13) indicate that our interpretations of the behaviour of the non-dimensional variables should not change with $Pr$, so the non-dimensional locations and intensities of flow features at different $Pr$ can be directly compared. Figure 12 depicts cross-sections of $\partial F/\partial\xi$ (related to vertical velocity as $\partial F/\partial\xi = -\nu^{-1/2}t^{1/2}w$) for $Pr = 0.5$ and $Pr = 5$. The maximum primary flow velocity and height of the maximum are shown in figure 13. The smaller-$Pr$ flow is much more vigorous and extensive, both vertically and laterally, than the larger-$Pr$ flow. Similar behaviour was also found in the flux-forced cases (not shown).

## 6. Concluding remarks

Horizontal free convection flows are abundant in nature and in engineering heat transfer problems. We investigated a particularly simple class of these flows: convection induced by a surface cooling that varied laterally as a step function with a step change. Similarity model solutions of the boundary-layer equations were obtained for flows of unstratified fluids driven by a surface buoyancy or buoyancy flux, and flows of stably stratified fluids driven by a surface buoyancy flux. The

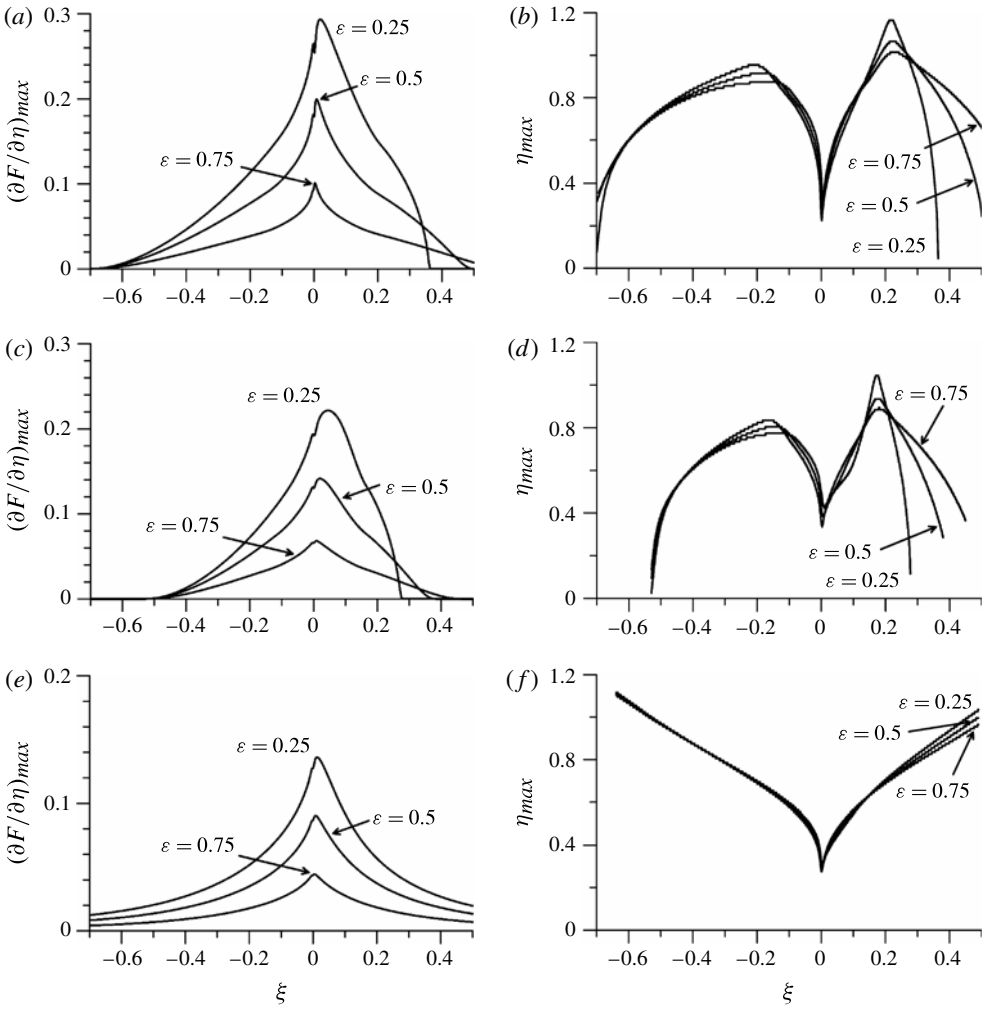


FIGURE 11. Sensitivity of the primary flow to $\varepsilon$ in cases UB (*a*,*b*), UF (*c*,*d*), and SF (*e*,*f*). Maximum horizontal velocity component $(\partial F/\partial\eta)_{max}$ (*a*,*c*,*e*) and height $\eta_{max}$ of that maximum (*b*,*d*,*f*) from the similarity model are shown as functions of the lateral coordinate $\xi$.

similarity-model predicted horizontal velocity fields were in very good agreement with the corresponding velocity fields obtained from numerical simulations in which no boundary-layer approximations were made. A similar comparison of the vertical velocity fields revealed larger discrepancies, although qualitatively good agreements were noted.

The fluid motion was characterized by a shallow, primarily horizontal flow capped by a weak return flow. In the unstratified fluid cases, the vertical motion (albeit weak compared to the horizontal motion in the primary flow) penetrated far above the developing momentum and buoyancy boundary layers. Stratification greatly suppressed this vertical motion. It also weakened the primary flow and strengthened the return flow.

The similarity models yielded power laws for the propagation speeds, trajectories and evolution of velocity maxima and other local extrema. For example, the peak

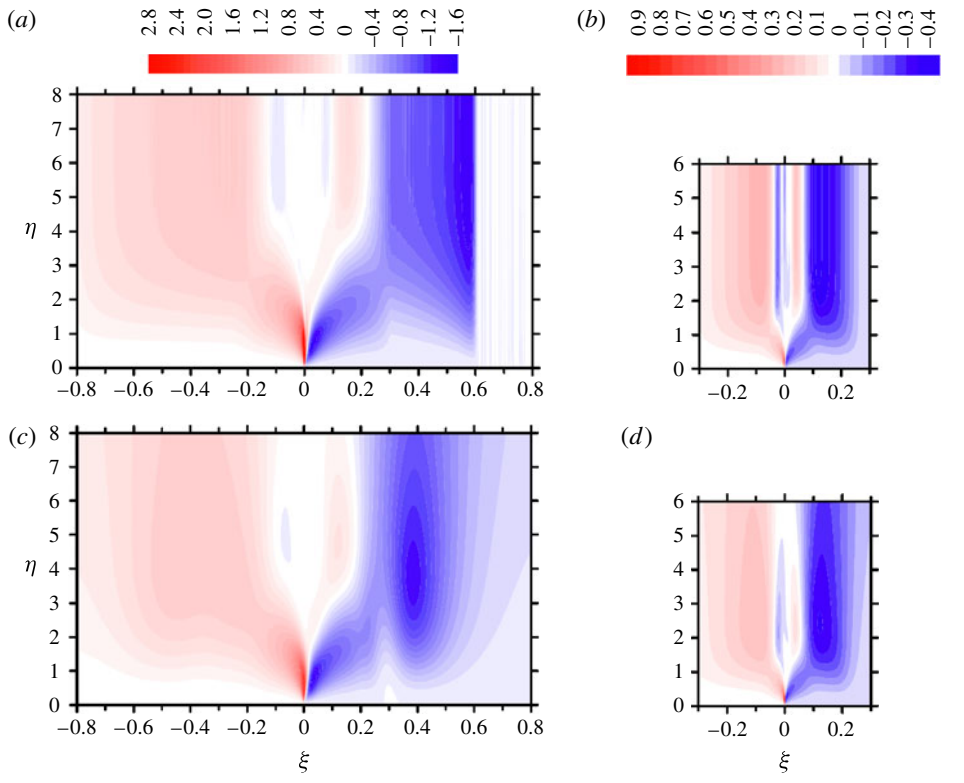


FIGURE 12. Vertical cross-sections of $\partial F/\partial\xi$ in case UB for ($a$,$c$) $Pr = 0.5$ and ($b$,$d$) $Pr = 5$, obtained from ($a$,$b$) the similarity model and ($c$,$d$) numerical simulation. The numerical plots are obtained from data output at $t = 975$ s in the $Pr = 0.5$ case and $t = 2041$ s in the $Pr = 5$ case.

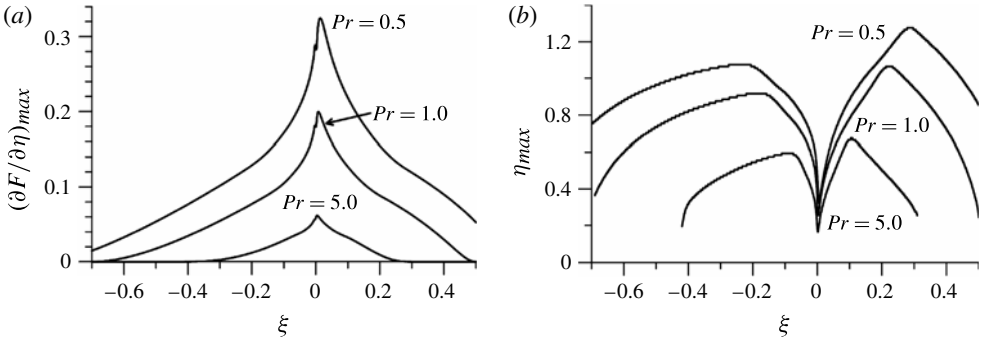


FIGURE 13. Sensitivity of the primary flow to $Pr$ in case UB. Similarity-model predicted maximum horizontal velocity component $(\partial F/\partial\eta)_{max}$ ($a$) and height $\eta_{max}$ of that maximum ($b$) as functions of the lateral coordinate $\xi$.

horizontal velocity component increased as $t^{1/4}$ in the unstratified buoyancy-forced case, and as $t^{1/2}$ in the flux-forced cases, regardless of stratification. In all cases the peak vertical velocity decreased as $t^{-1/2}$, and the depths of both momentum and buoyancy boundary layers grew as $t^{1/2}$.

The flows were strongly dependent on $Pr$, with the smaller-$Pr$ flows being more vigorous and spatially extensive. This can be understood by recalling that, as $x \to \pm\infty$, the problem reduced to that of diffusion in the vertical. The depth of the thermal boundary layer grew as $(\kappa t)^{1/2}$, which in non-dimensional form corresponds to $(T/Pr)^{1/2}$. Thus, at smaller $Pr$, the background buoyancy fields developed more quickly, and produced a stronger buoyancy contrast near the step change. The smaller-$Pr$ cases were thus associated with a stronger baroclinic forcing (from a vorticity dynamics perspective) and a stronger lateral pressure gradient force (from a pressure perspective).

It can be shown that if provision is made for the Coriolis force, non-hydrostatic terms, or lateral stress or diffusion terms, the governing equations are no longer invariant to the stretching transformation, and similarity models (if they exist) are not apparent. On the other hand, our similarity framework readily extends to flows of multi-component fluids driven by step changes in constituent concentrations or concentration fluxes at the surface. A related approach can also be applied to a description of wind-driven circulations in shallow coastal waters.

## REFERENCES


AMIN, N. & RILEY, N. 1990 Horizontal free convection. *Proc. R. Soc. Lond.* A **427**, 371–384.

ATKINSON, B. W. 1981 *Meso-Scale Atmospheric Circulations*. Academic.

BARENBLATT, G. I. 1996 *Scaling, Self-Similarity, and Intermediate Asymptotics*. Cambridge University Press.

BLUMAN, G. W. & COLE, J. D. 1974 *Similarity Methods for Differential Equations*. Springer.

CARSLAW, H. S. & JAEGER, J. C. 1959 *Conduction of Heat in Solids*, 2nd edn. Oxford University Press.

CHEN, T. S., TIEN, H. C. & ARMALY, B. F. 1986 Natural convection on horizontal, inclined, and vertical plates with variable surface temperature or heat flux. *Intl J. Heat Mass Transfer* **29**, 1465–1478.

CLIFTON, J. V. & CHAPMAN, A. J. 1969 Natural-convection on a finite-size horizontal plate. *Intl J. Heat Mass Transfer* **12**, 1573–1584.

DAYAN, A., KUSHNIR, R. & ULLMANN, A. 2002 Laminar free convection underneath a hot horizontal infinite flat strip. *Intl J. Heat Mass Transfer* **45**, 4021–4031.

DESWITA, L., NAZAR, R., AHMAD, R., ISHAK, A. & POP, I. 2009 Similarity solutions of free convection boundary layer flow on a horizontal plate with variable wall temperature. *Eur. J. Sci. Res.* **27**, 188–198.

DRESNER, L. 1983 *Similarity Solutions of Nonlinear Partial Differential Equations*. Pitman.

DRESNER, L. 1999 *Applications of Lie's Theory of Ordinary and Partial Differential Equations*. Institute of Physics.

EDE, A. J. 1967 Advances in free convection. In *Advances in Heat Transfer*, 4 (ed. J. P. Hartnett & T. F. Irvine Jr.), pp. 1–64. Academic.

FANNELØP, T. K. & WEBBER, D. M. 2003 On buoyant plumes rising from area sources in a calm environment. *J. Fluid Mech.* **497**, 319–334.

FEDOROVICH, E. & SHAPIRO, A. 2009*a* Structure of numerically simulated katabatic and anabatic flows along steep slopes. *Acta Geophys.* **57**, 981–1010.

FEDOROVICH, E. & SHAPIRO, A. 2009*b* Turbulent natural convection along a vertical plate immersed in a stably stratified fluid. *J. Fluid. Mech.* **636**, 41–57.

FUJII, T., HONDA, H. & MORIOKA, I. 1973 A theoretical study of natural convection heat transfer from downward-facing horizontal surfaces with uniform heat flux. *Intl J. Heat Mass Transfer* **16**, 611–627.

GARRATT, J. R. 1990 The internal boundary layer: a review. *Boundary-Layer Meteorol.* **50**, 171–203.

GEBHART, B., JALURIA, Y., MAHAJAN, R. L. & SAMMAKIA, B. 1988 *Buoyancy-Induced Flows and Transport*. Hemisphere.

GILL, W. N., ZEH, D. W. & DEL CASAL, E. 1965 Free convection on a horizontal plate. *Z. Angew. Math. Phys.* **16**, 539–541.

HIGUERA, F. J. 1998 Natural convection flow due to a heat source under an infinite horizontal surface. *Phys. Fluids* **10**, 3014–3016.

HUNT, G. R. & VAN DEN BREMER, T. S. 2010 Classical plume theory: 1937–2010 and beyond. *IMA J. Appl. Maths* **76** (3), 424–448.

INGHAM, D. B., MERKIN, J. H. & POP, I. 1986 Flow past a suddenly cooled horizontal plate. *Wärme-Stoffübertrag.* **20**, 237–241.

JABLONOWSKI, C. & WILLIAMSON, D. L. 2011 The pros and cons of diffusion, filters and fixers in atmospheric general circulation models. In *Numerical Techniques for Global Atmospheric Models* (ed. P. H. Lauritzen, C. Jablonowski, M. A. Taylor & R. D. Nair), pp. 389–504. Springer.

KAYE, N. B. 2008 Turbulent plumes in stratified environments: a review of recent work. *Atmos.-Ocean* **46** (4), 433–441.

MERKIN, J. H. 1985 A note on the similarity solutions for free convection on a vertical plate. *J. Engng Maths* **19**, 189–201.

MORTON, B. R., TAYLOR, G. I. & TURNER, J. S. 1956 Turbulent gravitational convection from maintained and instantaneous sources. *Proc. R. Soc. Lond.* A **234**, 1–23.

NEUFELD, J. A., GOLDSTEIN, R. E. & WORSTER, M. G. 2010 On the mechanisms of icicle evolution. *J. Fluid Mech.* **647**, 287–308.

OSTRACH, S. 1953 An analysis of laminar free-convection flow and heat transfer about a flat plate parallel to the direction of the generating body force. NACA *Tech. Rep.* no. 1111, pp. 63–79.

PERA, L. & GEBHART, B. 1973 Natural convection boundary layer flow over horizontal and slightly inclined surfaces. *Intl J. Heat Mass Transfer* **16**, 1131–1146.

ROTEM, Z. & CLAASSEN, L. 1969 Natural convection above unconfined horizontal surfaces. *J. Fluid Mech.* **38**, 173–192.

SAMANTA, S. & GUHA, A. 2012 A similarity theory for natural convection from a horizontal plate for prescribed heat flux or wall temperature. *Intl J. Heat Mass Transfer* **55**, 3857–3868.

SCASE, M. M., CAULFIELD, C. P., DALZIEL, S. P. & HUNT, J. C. R. 2006 Time-dependent plumes and jets with decreasing source strengths. *J. Fluid Mech.* **563**, 443–461.

SIMPSON, J. E. 1987 *Gravity Currents: In the Environment and the Laboratory*. Ellis Horwood.

SIMPSON, J. E. 1994 *Sea Breeze and Local Wind*. Cambridge University Press.

SINGH, S. N. & BIRKEBAK, R. C. 1969 Laminar free convection from a horizontal infinite strip facing downwards. *Z. Angew. Math. Phys.* **20**, 454–461.

SKAMAROCK, W. C. 2004 Evaluating mesoscale NWP models using kinetic energy spectra. *Mon. Weath. Rev.* **132**, 3019–3032.

SPARROW, E. M. & GREGG, J. L. 1958 Similar solutions for free convection from a non-isothermal vertical plate. *Trans. ASME* **80**, 379–386.

STEWARTSON, K. 1958 On the free convection from a horizontal plate. *Z. Angew. Math. Phys.* **9**, 276–282.

TURNER, J. S. 1962 The 'starting plume' in neutral surroundings. *J. Fluid Mech.* **13**, 356–368.

WOODS, A. W. 2010 Turbulent plumes in nature. *Annu. Rev. Fluid Mech.* **42**, 391–412.